2024 IEEE Ultrasonics, Ferroelectrics, and Frequency Control Joint Symposium (UFFC-JS) | 979-8-3503-7190-1/24/$31.00 ©2024 IEEE | DOI: 10.1109/UFFC-JS60046.2024.10793792

Coherence-Based Optimization Using Cumulative Spatial Lags to Estimate Sound Speed in Plane Wave Images of Coherent and Incoherent Targets

Jiaxin Zhang*, Yunlong Zhu†, and Muyinatu A. Lediju Bell*†§
*Department of Electrical and Computer Engineering, Johns Hopkins University, Baltimore, MD
†Department of Biomedical Engineering, Johns Hopkins University, Baltimore, MD
‡Department of Computer Science, Johns Hopkins University, Baltimore, MD

***Abstract*—A globally constant sound speed of 1540 m/s is often assumed when beamforming ultrasound images, despite variations in tissue properties that lead to different sound speeds. As a result, a globally constant sound speed that is not representative of the majority of local sound speeds can degrade image quality, resulting in inaccurate target depths, sizes, and shapes, thus reducing the overall effectiveness of diagnostic and interventional ultrasound imaging. In this paper, we developed a more general coherence-based optimization method to estimate sound speed that can be applied to both coherent and incoherent targets in ultrasound images with plane wave transmissions. Sound speeds that produced minimum values of the lateral full-width at half maximum (FWHM) of point targets and the contrast of anechoic targets were considered optimal. Our method estimated sound speeds that deviated from optimal values by 5-10 m/s. Our approach was benchmarked against a speckle brightness maximization approach, which achieved deviations of 57-160 m/s from the optimal sound speed values. The lower deviations with our approach resulted in a 46%-63% improvement in lateral FWHM and 1.09 dB contrast enhancement relative to the corresponding results of the speckle brightness maximization method. The proposed approach has the potential to improve accuracy in diagnostic and interventional ultrasound imaging.**

***Index Terms*—Sound speed estimation, spatial coherence, ultrasound beamforming, tissue characterization**

I. Introduction

In ultrasound beamforming, where the sound speed is often unknown, a default speed of 1540 m/s is commonly assumed, as this approximates the average velocity of ultrasound wave propagation in soft tissue [1]. However, the sound speed can vary significantly across different tissue types due to varying tissue properties [2]. The mismatch between the assumed and actual sound speeds can lead to degraded image quality, as well as inaccurate target depths, sizes, and shapes, which further decreases the accuracy and effectiveness of diagnostic and interventional ultrasound imaging [3], [4].

Previous work has employed various tissue-specific parameters to estimate sound speeds for ultrasound image formation, such as maximizing speckle brightness [5] or minimizing speckle size [6]. Sound speed errors of these speckle-related methods arise when the amplitude of a speckle region is maximized while other targets do not appear significantly changed or the selected regions have different tissue structures or are highly heterogeneous. Optimal sound speed can also be determined by maximizing the average coherence factor [7], [8], which offers advantages in computational efficiency and enhanced sensitivity to strong coherent reflectors. However, the coherence factor does not directly provide spatial correlations between individual channels, resulting in heightened sensitivity to acoustic reverberation artifacts which impact the accuracy of the coherence estimations [3], [9]–[11]. Imbault *et al.* [12] proposed maximizing the polynomial fit of the maximum spatial coherence to estimate sound speed in hepatic steatosis assessment. However, this method was proposed for estimation at a fixed focal depth in focused transmission ultrasound imaging and was not evaluated on plane wave ultrasound data.

Publicly available resources from the Challenge on Ultrasound Beamforming with Deep Learning (CUBDL) [13]–[15] provided standardized sound speeds using phantom data with plane wave transmissions and speckle brightness maximization [5]. Specifically, the corrected sound speed was selected as the one that maximized the average amplitude in a homogeneous region of speckle. However, we observed that some corrections only provide coarse improvement over the default speed of 1540 m/s in highly heterogeneous regions, which is consistent with the limitations noted above.

In this paper, we developed a spatial coherence-based optimization method to estimate sound speed in both coherent and incoherent targets. Our method does not require external devices for sound speed measurement or computations of tissue-specific parameters, and it can be applied to data acquired with plane wave transmissions. The contrast and full-width at half maximum (FWHM) were calculated for different target types to assess the improvement in image quality after applying the corrected sound speed determined by our method, using sound speeds derived from CUBDL phantom data as a benchmark.

II. Methods

Our sound speed estimation process is summarized in the flowchart presented in Fig. 1. Raw channel data acquired with plane wave transmissions were provided by the public CUBDL datasets [13]. Data sequences containing a phantom brain structure (i.e., INS012) and phantom vessel and wires (i.e., INS014), each with 75 transmission angles ranging -16° to 16°, were used in this work. Time delays were calculated at the default sound speed of 1540 m/s and applied to the

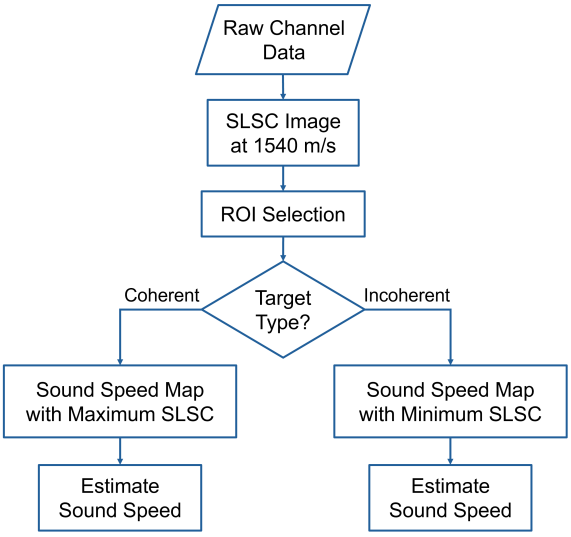

Fig. 1. Flowchart describing our coherence-based sound speed estimation method.

raw channel data. Spatial coherence, $\hat{R}$, was calculated by normalizing the covariance across the receive aperture by the variance of the signals from equally-spaced elements [9]:

$$\hat{R}(m) = \frac{1}{N-m} \sum_{i=1}^{N-m} \frac{\sum_{n=n_1}^{n_2} s_i(n) s_{i+m}(n)}{\sqrt{\sum_{n=n_1}^{n_2} s_i^2(n) \sum_{n=n_1}^{n_2} s_{i+m}^2(n)}} \tag{1}$$

where m is the spatial lag, in number of elements between two points in the aperture, N is the number of elements in the transducer, $s_i(n)$ is the time-delayed, zero-mean signal received at the ith element from the nth depth. The axial correlation kernel size, $n_2 - n_1$, was set to one wavelength. The short-lag spatial coherence (SLSC) pixel value was computed by summing the spatial coherence function across the first M lags [9]:

$$R_{sl} = \int_1^M \hat{R}(m) dm \approx \sum_{m=1}^{M} \hat{R}(m) \tag{2}$$

where M can range from 0% to 30% of the receive aperture.

For coherent targets, such as the point target in INS012 and the wire target in INS014, the backscattered pressure waves interfere constructively, resulting in higher coherence and thus brighter regions in SLSC images compared to the background. Sound speed maps were generated to visualize the maximum SLSC pixel values within a manually selected region of interest (ROI) in each SLSC image per sound speed per M.

For incoherent targets, such as the vessel in INS014, the destructive interference between ultrasound waves leads to reduced coherence, appearing as darker regions than the background in SLSC images. Sound speed maps for these targets were created by plotting the minimum SLSC pixel values within the target ROI in each SLSC image per sound speed per M.

The optimal sound speed at each M value was determined by either maximizing the maximum SLSC pixel value for coherent targets or minimizing the minimum SLSC pixel value for incoherent targets. The mode of the optimal sound speeds across the sound speed map was selected as the estimated sound speed within the target ROI.

To evaluate the visibility of the selected image targets relative to their background in delay-and-sum (DAS) images, contrast was computed as follows:

$$\text{Contrast} = 20 \log_{10} \left(\frac{\mu_t}{\mu_b} \right) \tag{3}$$

where μ_t and μ_b are the mean beamformed signals (i.e., after envelope-detection and prior to log compression) within the target and background ROIs, which were placed at the same depth inside and outside the target, respectively. To determine lateral resolution, the lateral FWHM of point targets was measured. Depending on the image target, either contrast or lateral FWHM was plotted as a function of sound speed. The optimal image quality was determined by the minimum lateral FWHM for point targets or the minimum contrast for anechoic targets. Sound speeds estimated by our proposed method were benchmarked with those corrected by speckle brightness maximization, which was implemented to standardized the sound speeds in CUBDL phantom data. These sound speeds were additionally compared to those associated with the optimal image quality.

III. Results and Discussion

Fig. 2 shows DAS images after beamforming with the sound speeds annotated at the top of each image. In the top row, we observe clearer brain structure edges and better image resolution with the 1380 m/s estimated by our method, when compared to images created with 1540 m/s and 1535 m/s, which are the default sound speed and the corrected speed provided by CUBDL, respectively. In the bottom row, although our method provides different estimated sound speeds of 1480 m/s and 1495 m/s for the vessel and wire targets, respectively, the corresponding DAS images reconstructed with these two sound speeds show reduced acoustic clutter inside the vessel, improved contrast between the vessel and its surroundings, and better separation between wire targets when compared to images created with the default sound speed (1540 m/s) and the corrected sound speed provided by CUBDL (1542 m/s).

Fig. 3 shows image quality metrics plotted as a function of sound speed. In Fig. 3(a), the lateral resolution of a point target in the INS012 phantom was optimized at a sound speed of 1375 m/s, with the minimum lateral FWHM measuring 0.46 mm. Our method produced a sound speed that deviated from this value by 5 m/s, while the CUBDL sound speed deviated by 160 m/s, yielding corresponding lateral FWHMs of 0.48 mm and 1.29 mm, respectively, resulting in a resolution improvement of 62.79% with the sound speed estimated by our method compared to that corrected by CUBDL. Similarly, in Fig. 3(b), lateral resolution was optimized at a sound speed of 1485 m/s with a lateral FWHM value of 0.42 mm when

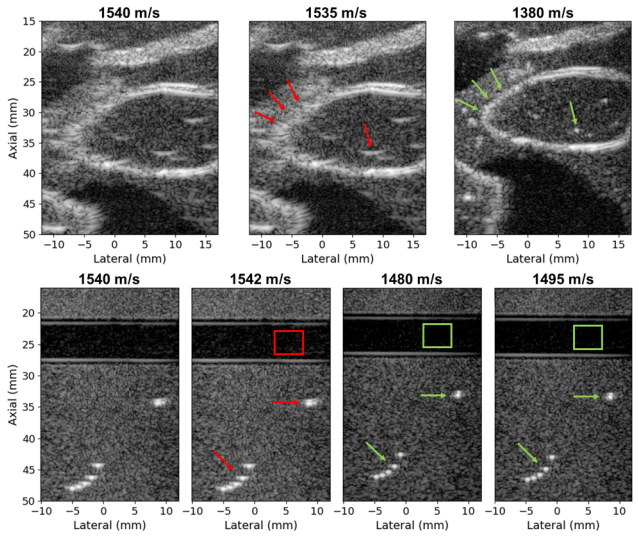

Fig. 2. (top) INS012 phantom images of brain structure at default sound speed, CUBDL sound speed, and our sound speed from left to right. (bottom) INS014 phantom images of vessel and wires at default sound speed, CUBDL sound speed, our sound speed of vessel and our sound speed of wire from left to right. Images are displayed with 60 dB dynamic range.

imaging a point target in the INS014 phantom acquisition. Sound speeds estimated by our method and by CUBDL deviated from this sound speed by 10 m/s and 57 m/s, respectively, corresponding to lateral FWHM values of 0.42 mm and 0.78 mm, respectively, resulting in a 46.15% improvement in the resolution achieved at the sound speed determined by our method relative to that achieved by CUBDL. In Fig. 3(c), the contrast of the vessel in the INS014 phantom acquisition was optimized at a sound speed of 1475 m/s, with the contrast measuring -20.04 dB. Our estimated sound speed and the CUBDL sound speed deviated from the optimal speed by 5 m/s and 67 m/s, respectively, corresponding to contrast values of -20.02 dB and -18.93 dB, respectively (i.e., a 1.09 dB enhancement in image contrast obtained at our estimated sound speed compared to the contrast obtained with the sound speed provided by CUBDL).

In the three example comparisons provided in Fig. 3, the sound speeds estimated with our method were consistently closer to those that produced optimal image quality when compared to sound speeds estimated using speckle brightness maximization. The acoustic clutter [16] in the anechoic regions of images is also visibly reduced with our method when compared to the images produced with 1540 m/s or the sound speeds provided by CUBDL. These results demonstrate the effectiveness of the proposed coherence-based approach to determine sound speeds for both coherent and incoherent regions, without requiring calculations of various image quality metrics to optimize the appearance of corresponding targets. Future work will apply our proposed approach to *in vivo* cases.

IV. Conclusion

This paper is the first to present a spatial coherence-based optimization method to estimate sound speeds in ultrasound

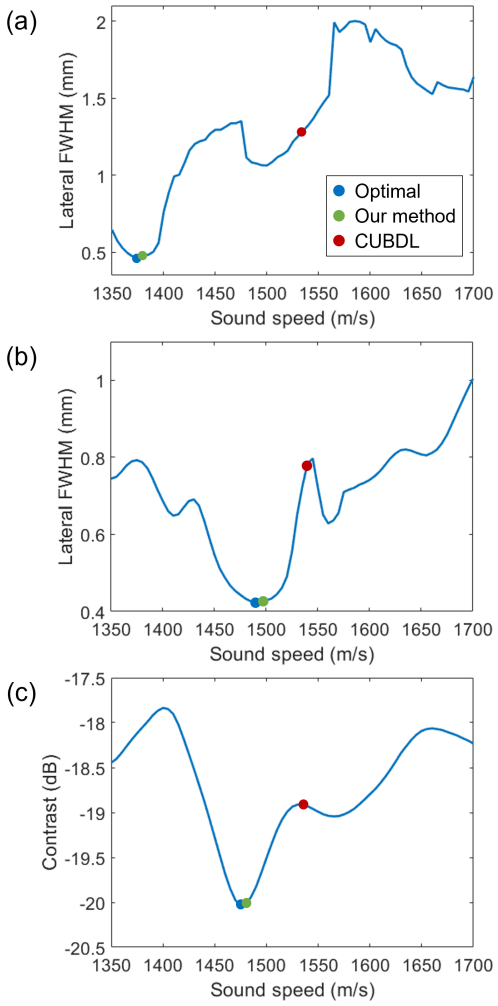

Fig. 3. (a) Lateral FWHM plot of a point target in the brain structure in INS012 phantom. (b) Lateral FWHM plot of a wire target and (c) contrast plot of a vessel region in INS014 phantom.

imaging with plane wave transmissions that is applicable to both coherent and incoherent targets. Compared to a speckle brightness maximization approach, our method resulted in images with clearer target boundaries, reduced acoustic clutter, 46%-63% improved lateral resolution, and 1.09 dB improved contrast. The sound speeds estimated with our approach deviated from sound speeds that maximized resolution and contrast by 5-10 m/s and from sound speeds based on maximum speckle brightness (i.e., CUBDL sound speeds) by 57-160 m/s. The proposed coherence-based approach to sound speed estimation is promising for *in vivo* applications and improving accuracy in diagnostic and interventional ultrasound imaging.

V. Acknowledgement

This work is supported by NSF SCH Award IIS 2014088 and NIH R01 EB032960.

REFERENCES

[1] T. L. Szabo, *Diagnostic ultrasound imaging: inside out*. Academic Press, 2013.

[2] L. Nock, G. E. Trahey, and S. W. Smith, "Phase aberration correction in medical ultrasound using speckle brightness as a quality factor," *The Journal of the Acoustical Society of America*, vol. 85, no. 5, pp. 1819–1833, 1989.

[3] W. F. Walker and G. E. Trahey, "A fundamental limit on delay estimation using partially correlated speckle signals," *IEEE Transactions on Ultrasonics, Ferroelectrics, and Frequency Control*, vol. 42, no. 2, pp. 301–308, 1995.

[4] Q. Chen and J. A. Zagzebski, "Simulation study of effects of speed of sound and attenuation on ultrasound lateral resolution," *Ultrasound in Medicine & Biology*, vol. 30, no. 10, pp. 1297–1306, 2004.

[5] M. Anderson, M. McKeag, and G. Trahey, "The impact of sound speed errors on medical ultrasound imaging," *The Journal of the Acoustical Society of America*, vol. 107, no. 6, pp. 3540–3548, 2000.

[6] X. Qu, T. Azuma, J. T. Liang, and Y. Nakajima, "Average sound speed estimation using speckle analysis of medical ultrasound data," *International Journal of Computer Assisted Radiology and Surgery*, vol. 7, pp. 891–899, 2012.

[7] H. Hasegawa and R. Nagaoka, "Initial phantom study on estimation of speed of sound in medium using coherence among received echo signals," *Journal of Medical Ultrasonics*, vol. 46, pp. 297–307, 2019.

[8] R. Ali, A. V. Telichko, H. Wang, U. K. Sukumar, J. G. Vilches-Moure, R. Paulmurugan, and J. J. Dahl, "Local sound speed estimation for pulse-echo ultrasound in layered media," *IEEE Transactions on Ultrasonics, Ferroelectrics, and Frequency Control*, vol. 69, no. 2, pp. 500–511, 2021.

[9] M. A. Lediju, G. E. Trahey, B. C. Byram, and J. J. Dahl, "Short-lag spatial coherence of backscattered echoes: Imaging characteristics," *IEEE Transactions on Ultrasonics, Ferroelectrics, and Frequency Control*, vol. 58, no. 7, pp. 1377–1388, 2011.

[10] J. J. Dahl, D. Hyun, M. A. Lediju, and G. E. Trahey, "Lesion detectability in diagnostic ultrasound with short-lag spatial coherence imaging," *Ultrasonic Imaging*, vol. 33, no. 2, pp. 119–133, 2011.

[11] A. Sharma, E. Oluyemi, K. Myers, E. Ambinder, and M. A. L. Bell, "Spatial coherence approaches to distinguish suspicious mass contents in fundamental and harmonic breast ultrasound images," *IEEE Transactions on Ultrasonics, Ferroelectrics, and Frequency Control*, vol. 71, no. 1, pp. 70–84, 2024.

[12] M. Imbault, A. Faccinetto, B.-F. Osmanski, A. Tissier, T. Deffieux, J.-L. Gennisson, V. Vilgrain, and M. Tanter, "Robust sound speed estimation for ultrasound-based hepatic steatosis assessment," *Physics in Medicine & Biology*, vol. 62, no. 9, p. 3582, 2017.

[13] M. A. L. Bell, J. Huang, A. Wiacek, P. Gong, S. Chen, A. Ramalli, P. Tortoli, B. Luijten, M. Mischi, O. M. H. Rindal, V. Perrot, H. Liebgott, X. Zhang, J. Luo, E. Oluyemi, and E. Ambinder, "Challenge on Ultrasound Beamforming with Deep Learning (CUBDL) Datasets," 2019.

[14] D. Hyun, A. Wiacek, S. Goudarzi, S. Rothlübbers, A. Asif, K. Eickel, Y. C. Eldar, J. Huang, M. Mischi, H. Rivaz, D. Sinden, R. J. G. van Sloun, H. Strohm, and M. A. L. Bell, "Deep learning for ultrasound image formation: CUBDL evaluation framework and open datasets," *IEEE Transactions on Ultrasonics, Ferroelectrics, and Frequency Control*, vol. 68, no. 12, pp. 3466–3483, 2021.

[15] M. A. L. Bell, J. Huang, D. Hyun, Y. C. Eldar, R. Van Sloun, and M. Mischi, "Challenge on ultrasound beamforming with deep learning (cubdl)," in *Proceedings of the IEEE International Ultrasonics Symposium (IUS)*, pp. 1–5, IEEE, 2020.

[16] M. A. Lediju, M. J. Pihl, J. J. Dahl, and G. E. Trahey, "Quantitative assessment of the magnitude, impact and spatial extent of ultrasonic clutter," *Ultrasonic Imaging*, vol. 30, no. 3, pp. 151–168, 2008.